JOURNAL OF SOLID STATE CHEMISTRY 14, 229–237 (1975)

On the Crystal Structures of the Fluorite-Related Intermediate Rare-Earth Oxides

PETER KUNZMANN* AND LEROY EYRING†

Department of Chemistry, Arizona State University, Tempe, Arizona 85281

Received July 18, 1974; revised September 26, 1974

The binary oxides of the rare-earth elements are, except for the *A*- and *B*-type sesquioxides, members of a fluorite-related homologous series R_nO_{2n-2} ($n = 4, 6, 7, 9, 10, 11, 12, \infty$ are well established and a related phase with $n = 10\frac{1}{2}$ has been reported). In this paper an electron optical study of members of the series is discussed which reveals the unit cell dimensions and possible space groups of the intermediate phases as well as the transformation matrices in terms of the fluorite substructure. This information reveals the structural relationships among the members of the series as well as the highest common structural feature involved. Structures are proposed for members of this series consistent with the new results obtained and with the data already in existence.

Introduction

The occurrence of an homologous series of intermediate phases in all the fluorite-related rare-earth oxides with the generic formula R_nO_{2n-2} has long since been reviewed (*1*). (R symbolizes either Ce, Pr or Tb, and n is an integer between 4 and ∞.) These intermediate phases have well-defined stoichiometries and ordered structures. Table I lists the established members of the series in the PrO_x and TbO_x systems.

The parent crystal structure for all these phases is the face-centered cubic fluorite structure which is formed by many dioxides. It can be visualized as a simple cubic arrangement of oxygen atoms with metal atoms being located in every second cubic hole giving a three-dimensional chessboard framework. The coordination sphere of oxygen is a tetrahedral arrangement of four metal atoms and the metal atoms are surrounded by eight oxygen atoms forming a cube.

X-ray powder diffraction studies (*2*) clearly demonstrated the structural relationship of the homologous series to fluorite: the structures of all intermediate phases were shown to be derivable from the fluorite structure of the dioxide by the introduction of oxygen vacancies in some ordered arrangement. The vacancies thus form a superlattice imposed on the basic lattice with the fluorite structure.

Unfortunately, the powder patterns showed only a few weak superstructure reflections such that the true superstructure lattice parameters could not be determined except in the case of the iota phase (R_7O_{12}). The splitting of the strong reflections, however, indicated the kind of distortion that the basic lattice experienced and the concomitant lowering of the symmetry.

Single crystals of an intermediate phase were prepared and X-ray diffraction data collected only in the case of the beta phase ($Pr_{12}O_{22}$) (*3*). Attempts to determine the vacancy arrangement from single crystal X-ray diffraction studies resulted in the discovery of a number of problems which may well make this path impassable. The intensities of the superstructure reflections are dominated by metal

* Present address: Schweizerische Aluminium AG, Forschungszentrum Neuhausen a/Rheinfall, Switzerland.

† Author to whom inquiries should be addressed.

TABLE I

MEMBERS OF THE HOMOLOGOUS SERIES IN THE PrO_x AND TbO_x SYSTEMS

n	Name	Composition x	Fraction of oxygen atoms missing	PrO_x system	TbO_x system
4	Sesquioxide	1.500	1/4	Pr_2O_3	Tb_2O_3
7	Iota	1.714	1/7	Pr_7O_{12}	Tb_7O_{12}
9	Zeta	1.778	1/9	Pr_9O_{16}	
10	Epsilon	1.800	1/10	$Pr_{10}O_{18}$	
11	Delta	1.818	1/11	$Pr_{11}O_{20}$	$Tb_{11}O_{20}$
12	Beta	1.833	1/12	$Pr_{12}O_{22}$	
∞	Dioxide	2.000	0	PrO_2	TbO_2

atom shifts which have to be refined in order to phase the superstructure reflections. This is not trivial because any refinement has to start from a set of qualitatively correct shifts, which have to be found by some other means. Absorption is serious particularly for a crystal large enough to yield superstructure reflections sufficiently strong to be recorded with reasonable accuracy. Twinning, observed in most cases, makes valid absorption corrections impossible without which a refinement of the metal atom shifts can never yield the low and reliable R-value needed as a criterion of the correctness of the model for the metal atom shifts.

Because of these difficulties a different approach to the problem of determining the structures has been utilized. Any relationship between the intermediate structures besides their being derivable from the fluorite structure e.g., a relationship between their superstructures, would be manifest in a formal relationship between the superstructure lattice parameters of the intermediate phases. Superstructure lattice parameters were therefore determined from electron diffraction patterns taken in a high resolution transmission electron microscope from very small single crystals (average size: 1 μm). A formal relationship did, in fact, appear as a certain periodicity occurring in the structures of all members of the homologous series listed in Table I at least in one direction. Corresponding features of the δ' phase ($TbO_{1.809}$) were also observed. The structural principle related to this axis was found from an inspection of the known iota structure and structural models for other phases were derived on this basis.

Experimental Part

Specimen Preparation

$Tb_{12}O_{22}$ crystals were obtained as a by-product in a hydrothermal run (*3*) which yielded $Tb_{11}O_{20}$ as the major product. For specific reaction conditions see the paragraph following.

$Tb_{11}O_{20}$ crystals were the major product of hydrothermal treatment of a charge of 0.092 g of TbO_x-powder and 0.100 g of concentrated HNO_3 which was heated in a sealed gold capsule to 820°C at a pressure of 23 000 psi. When these conditions were achieved the pressure was slowly lowered to 16 500 psi over 24 hr. The system was then cooled to room temperature in 3 hr and the pressure lowered to 1 atm.

$TbO_{1.809}$ (δ' phase) crystals were obtained when a large crystalline sample of TbO_x was heated to 1000°C *in vacuo* (in order to convert it to the sesquioxide) and then cooled to 475°C, where it was annealed in an oxygen pressure of 400 Torr for 20 hr and finally cooled rapidly to room temperature.

$Pr_{12}O_{22}$ crystals were obtained as described previously (*3*).

$Pr_{10}O_{18}$. A sample of coarse crystalline PrO_2 was heated to 1000°C *in vacuo* (to convert it to the sesquioxide), annealed at 565°C and 13.5 Torr for 24 hr then cooled rapidly to room temperature.

Pr_9O_{16}. The same procedure was used as for preparing $Pr_{10}O_{18}$ except that the annealing occurred at 580°C and 12.5 Torr O_2 or at 600°C and 16.5 Torr O_2.

Electron Optical Studies

The electron diffraction patterns of each of the phases were taken on a JEM 100B electron microscope with a 30°-tilting stage. The patterns (a representative few are shown in Fig. 1) show strong basic fluorite reflections and weak superstructure reflections in rows between two basic reflections. These rows have multiplicities characteristic of each phase related in a simple way to its n-value (i.e., 7 for R_7O_{12}, 9 for R_9O_{16}, 11 for $R_{11}O_{20}$, 20 or any of its common dividers for $R_{10}O_{18}$, 12 or any of its common dividers for $Pr_{12}O_{22}$, 24 or any of its common dividers for $Tb_{12}O_{22}$ and 31 for $TbO_{1.809}$ (δ' phase)). Since each of the

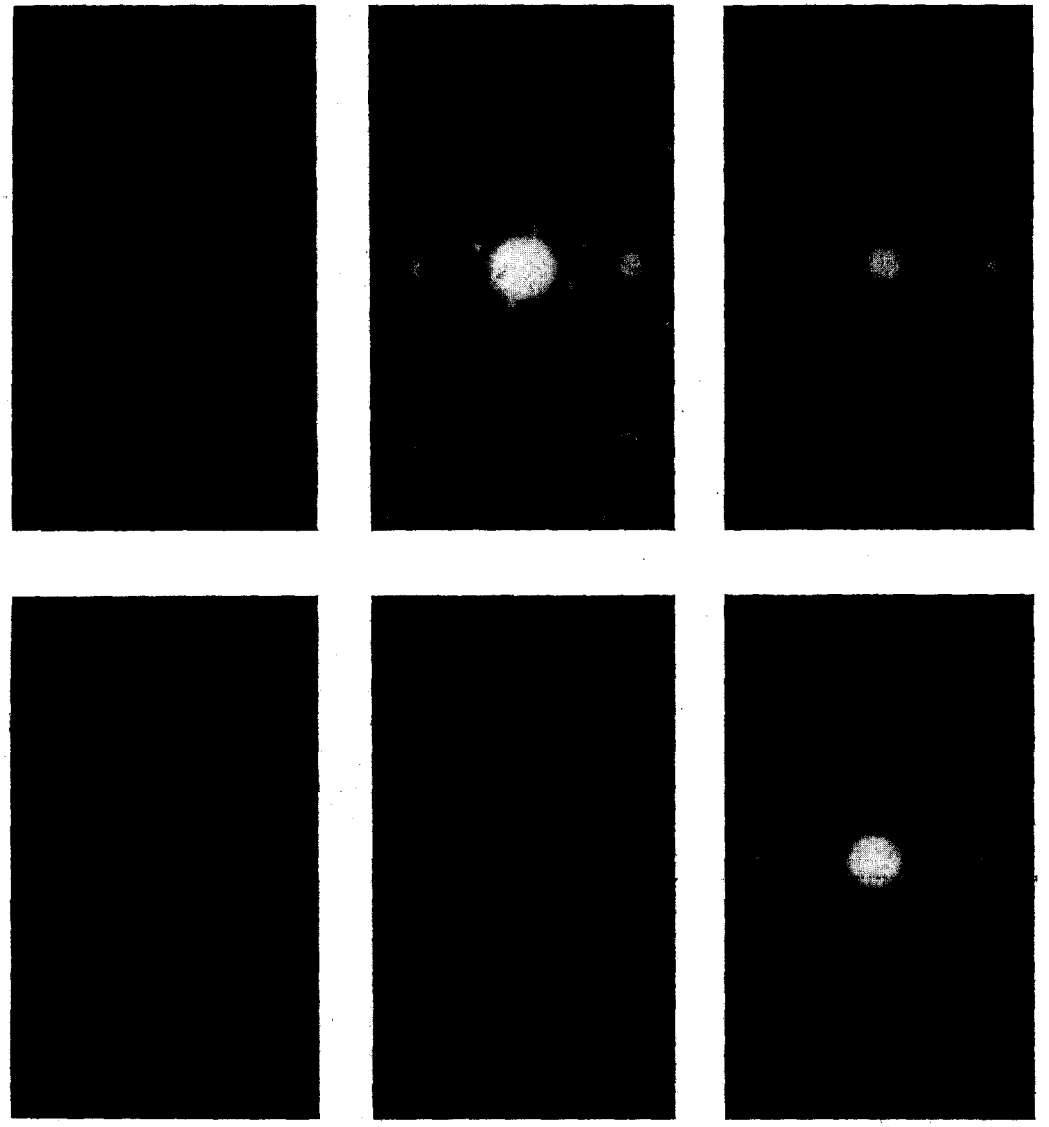

FIG. 1. Electron diffraction patterns of members of the homologous series of rare earth oxides in the $\langle 21\bar{1}\rangle_F$ zone.

phases, except δ', has at least one real axis along $[211]_F$, each of them has at least one $\langle 211\rangle_F$ zone in the reciprocal lattice as a low-index zone in terms of the superstructure lattice. The superstructure lattice parameters were determined by exploring the whole three-dimensional reciprocal lattice by taking several sections through it. Reciprocal axes were then chosen for the superstructure and all reflections indexed according to that choice. The basic reflections could thus be indexed in terms of the basic lattice as well as in terms of the superstructure lattice. This relationship yielded a transformation matrix, the inverse transpose matrix of which yielded the relationship of the superstructure unit cell parameters to the basic structure unit cell parameters. Ideal lattice parameters, not taking any distortions of the basic lattice into account, were determined using this relationship.

The technique of lattice imaging was applied according to procedures developed by Cowley and Iijima (*4*) who have given a theoretical and experimental justification that pictures obtained with this method can be interpreted directly in terms of a structural model provided certain conditions are met. These include a maximum thickness of the crystal under examination of ~150 Å, an accurate alignment of the crystal to within a fraction of a degree and an optimum underfocus of about 900 Å. The technique uses several diffracted beams with or without inclusion of the primary beam to form the image. Interference of these beams with each other results in a contrast pattern in the image which not only has the periodicity and symmetry of the crystal structure but also contains information on the structure within the unit cell.

An optical diffractometer was used to enhance the micrographs obtained. In this technique a laser beam is scattered by the micrograph producing a diffraction pattern containing the spots belonging to any periodic pattern plus diffuse background. If a template is cut that permits only the sharp reflections to pass through and absorbs all diffuse background, an image can be reconstructed which shows the periodic pattern without the superimposed noise. The apparatus used was similar to that described by Markham (*5*). In addition a polarizing filter was inserted to reduce the intensity to a convenient value.

Lattice Parameters and Derivation of a Formal Relationship

Table II lists the lattice parameters and some relevant information derivable from them for all intermediate phases investigated. The lattice parameters are those derived from the basic lattice except where refined values are available from other studies (*3, 6*). The relative volume is the ratio of the unit cell volume of the superstructure to the basic structure. The composition of $Tb_{12}O_{22}$ has not been positively confirmed, but all evidence suggests it is correct as will be further indicated below. The space group *Pn* has not been confirmed but is set by analogy to $Pr_{12}O_{22}$.

Each intermediate phase, except $TbO_{1.809}$ (δ' phase), has at least one axis of the kind $(a_f + \frac{1}{2}b_f - \frac{1}{2}c_f)$ which we shall subsequently refer to as the vector $\frac{1}{2}[21\bar{1}]$. This periodicity occurs three times for R_7O_{12}, twice for Pr_9O_{16} and $R_{11}O_{20}$, and once for $Pr_{10}O_{18}$, $Pr_{12}O_{22}$, and $Tb_{12}O_{22}$.

Furthermore, the two $\frac{1}{2}[21\bar{1}]$ axes of δ and ζ and two of the three axes of ι have the same orientational relationship with each other. These three structures therefore have one plane in common and differ only in the third axis. The structures of $Pr_{10}O_{18}$, $Pr_{12}O_{22}$ and $Tb_{12}O_{22}$ also have a plane in common which is given by their *a*- and *c*-axes. It is a different plane, however, than that common to the odd numbered members mentioned above and is parallel to a glide plane which determines the monoclinic symmetry. The δ'-structure has no such relationship to the other structures.

Structural Relationships and the Deduction of Structural Models

Conclusions Possible from Electron Diffraction

R_7O_{12}. Ordered phases of R_7O_{12} are found in several binary as well as ternary oxide systems. Baenziger et al. (*7*) determined the correct superstructure symmetry and lattice parameters for the binary Tb_7O_{12}. Bartram (*8*) has determined the structure of the isomorphous UY_6O_{12}. Two oxygen vacancies

TABLE II

STRUCTURAL DATA ON INTERMEDIATE RARE EARTH OXIDE PHASES

Composition	n (in R_nO_{2n-2})[a]	Symmetry	Lattice parameters	Relation to basic structure	Relative volume	No. of vacancies/ unit cell
$RO_{1.500}$	4	$Ia\bar{3}$	$a = 11.152$ Å ($PrO_{1.5}$) $a = 10.728$ Å ($TbO_{1.5}$)	$a = 2a_f$	8	16
$RO_{1.714}$	7	$R\bar{3}$	$a = 6.750$ Å, $\alpha = 99°23'$ ($PrO_{1.714}$) $a = 6.509$ Å, $\alpha = 99°21'$ ($TbO_{1.714}$)	$a = a_f + \frac{1}{2}b_f - \frac{1}{2}c_f$	7/4	2
$PrO_{1.778}$	9	Triclinic	$a = 6.5$ Å $b = 8.4$ Å $c = 6.5$ Å $\alpha = 97.3°$ $\beta = 99.6°$ $\gamma = 75.0°$	$a = a_f + \frac{1}{2}b_f - \frac{1}{2}c_f$ $b = \frac{3}{2}b_f + \frac{1}{2}c_f$ $c = \frac{1}{2}a_f - \frac{1}{2}b_f + c_f$	9/4	2
$PrO_{1.800}$	10	Pn	$a = 6.7$ Å $b = 19.3$ Å $c = 15.5$ Å $\beta = 125.2°$	$a = a_f + \frac{1}{2}b_f - \frac{1}{2}c_f$ $b = \frac{5}{2}(-b_f - c_f)$ $c = 2(-b_f + c_f)$	10	8
$TbO_{1.809}$	$10\frac{1}{3}$	Triclinic	$a = 13.8$ Å $b = 16.2$ Å $c = 12.1$ Å $\alpha = 107.4°$ $\beta = 100.1°$ $\gamma = 92.2°$	$a = -\frac{1}{2}a_f + \frac{5}{2}c_f$ $b = -2a_f - 2b_f - c_f$ $c = 2a_f - b_f$	31/2	12
$RO_{1.818}$	11	Triclinic	$a = 6.5$ Å $b = 9.9$ Å $c = 6.5$ Å $\alpha = 90.0°$ $\beta = 99.6°$ $\gamma = 96.3°$	$a = a_f + \frac{1}{2}b_f - \frac{1}{2}c_f$ $b = -\frac{1}{2}a_f + \frac{3}{2}b_f + c_f$ $c = \frac{1}{2}a_f - \frac{1}{2}b_f + c_f$	11/4	2
$TbO_{1.833}$	12	Pn	$a = 6.7$ Å $b = 23.2$ Å $c = 15.5$ Å $\beta = 125.2°$	$a = a_f + \frac{1}{2}b_f - \frac{1}{2}c_f$ $b = 3(-b_f - c_f)$ $c = 2(-b_f + c_f)$	12	8
$PrO_{1.833}$	12	Pn	$a = 6.687$ Å $b = 11.602$ Å $c = 15.470$ Å $\beta = 125°15'$	$a = a_f + \frac{1}{2}b_f - \frac{1}{2}c_f$ $b = \frac{3}{2}(-b_f - c_f)$ $c = 2(-b_f + c_f)$	6	4
$RO_{2.000}$	∞	$Fm3m$	$a = 5.393$ Å (PrO_2) $a = 5.220$ Å ($TbO_{1.95}$)		1	0

[a] If a phase occurs in the PrO_x as well as in the TbO_x system R is used, otherwise the specific symbol is used.

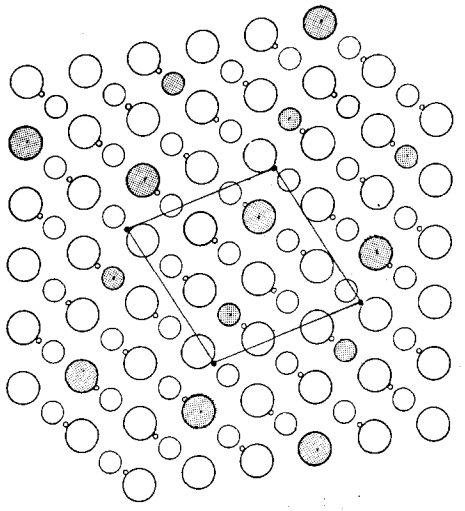

FIG. 2. Projection of the iota structure along $[100]_I = [21\bar{1}]_F$. Small circles represent rows of metal atoms—larger circles mark rows of oxygen positions. The shaded circles represent oxygen vacancies.

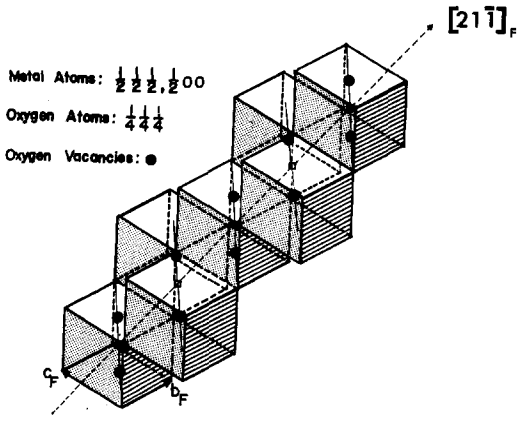

FIG. 3. Arrangement of vacancy pairs along the a axis, $[21\bar{1}]_F$ common to members of the homologous series.

are accommodated along the threefold axis of the rhombohedral unit cell. This is, in fact, the only possible arrangement of vacancies. An inspection of the rhombohedral space group $R\bar{3}$ shows that twofold positions occur only along the threefold axis. Since the basic lattice contains only two oxygen positions per unit cell there is only one possible way of removing two oxygen atoms and thus forming two vacancies along that axis. The structure is shown in Fig. 2. in projection along one of the rhombohedral axes.

The strings of vacancy pairs thus formed along $[111]_F$ also occur in the *bcc* sesquioxide structure. They do not occur, however, in any of the other intermediate phases discussed here as can easily be rationalized by inspection of their superstructure unit cell parameters, none of which has a periodicity along any of the $\langle 111\rangle_F$ axes. The arrangement of vacancies along each of the three rhombohedral axes which are all vectors of the kind $\frac{1}{2}[21\bar{1}]$ with respect to the basic lattice, is shown in Fig. 3. It is postulated to be the element common to all intermediate phases, except the δ'-$TbO_{1.809}$. It is not considered as a structural unit which can be recognized as a separate entity in these structures. Rather, it is considered as a structural principle which dictates the arrangement of vacancy doublets in a certain direction.

Pr_9O_{16} and $R_{11}O_{20}$. These phases both have two $\frac{1}{2}[21\bar{1}]$ axes in common with the iota structure. If we accept the hypothesis that the arrangement of vacancies along these axes should always be the same, the construction of the ζ and δ structures is straightforward. Planes of vacancy doublets parallel to the a- and c-axes, having the same two-dimensionally periodic structure as occurs in the iota structure, are stacked together with the distance and orientation appropriate to the b-axis. A projection of the resultant structure of δ is shown in Fig. 4.

$Pr_{10}O_{18}$, $Pr_{12}O_{22}$ and $Tb_{12}O_{22}$. The formal relationship between these structures suggests that they are built of identical layers perpendicular to b. $Pr_{12}O_{22}$ has four vacancies per unit cell, which can be accounted for by two vacancy pairs related by the glide plane. The orientation of the pairs is given by the fact that the a-axis is of the $\frac{1}{2}[21\bar{1}]$ type and that the arrangement of the vacancies along this axis should, therefore, be that of Fig. 3. It is interesting that the two different vacancy pair orientations, related by the glide plane, both have the relationship with the a-axis given in Fig. 3. That still leaves one degree of freedom: the distance of the vacancy pairs to the glide-plane. As a result of this, two different structures can be constructed. All information

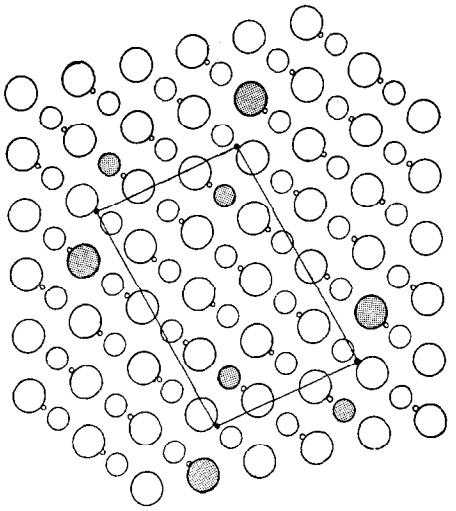

FIG. 4. Projection of the delta structure along the $[001]_\delta = [21\bar{1}]_F$.

presently available is, however, insufficient to decide which is correct. The structure of $Pr_{12}O_{22}$, therefore, remains ambiguous.

The structure of $Pr_{10}O_{18}$ is made up of two layers per periodic displacement along *b* since the unit cell contains four vacancy pairs. The two layers must be rotated with respect to each other, otherwise the periodicity along *b* would be half that observed. The distance between them is fixed by the value of *b*, but there are still several ways of stacking them together. This translational relationship is another degree of freedom which could not be determined unambiguously.

The observation of a double-layered structure for $Pr_{10}O_{18}$ suggests a similar situation for β-$TbO_{1.833}$, which would confirm its stoichiometry.

δ'-$TbO_{1.809}$. A thermodynamic characterization of this phase, although incomplete, unambiguously confirms a rather narrow compositional region of stability corresponding to a nonintegral *n*-value of $10\frac{1}{3}$ (*9*). The lattice parameters do not show any relationship to those of the other intermediate phases. This phase, therefore, does not really belong to the homologous series. Its structure with triclinic symmetry and 12 vacancies per unit cell, related at the most by a center of symmetry, is certainly the most complex encountered so far in this system.

The correlation of the lattice vectors for all

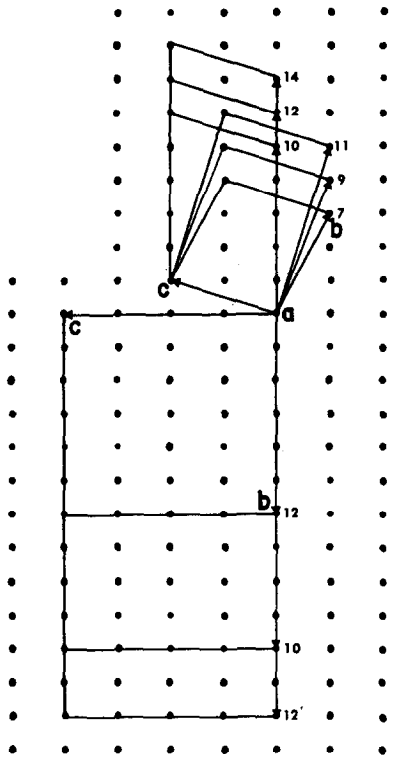

FIG. 5. Projections of the unit cells of members of the homologous series along the common *a* axis, $[21\bar{1}]_F$.

the phases discussed except for δ' are shown in Fig. 5 in projection along the *a*-axis which is common to all. Also indicated are the vectors of the γ-$Zr_5Sc_2O_{13}$ ($Zr_{10}Sc_4O_{26}$) lattice (*10*) and some other possible triclinic even-members of the homologous series.

Evidence Provided by Lattice Imaging

The technique of lattice imaging has been utilized using thin crystals of $Tb_{11}O_{20}$. In the rare earth oxide structures the superstructure consists of oxygen vacancies altered by shifted metal and oxygen positions and therefore would not be expected to produce as wide contrast as if there were interstitial heavy metal atoms involved. However, it should be possible to detect the periodicities imposed on the structure by the vacancies. A bright field image on which the unit cell is projected and on which the diffraction pattern is inset is reproduced in Fig. 6. The regularity of two light spots per unit cell in this projection is striking particularly in the lower part of Fig. 6

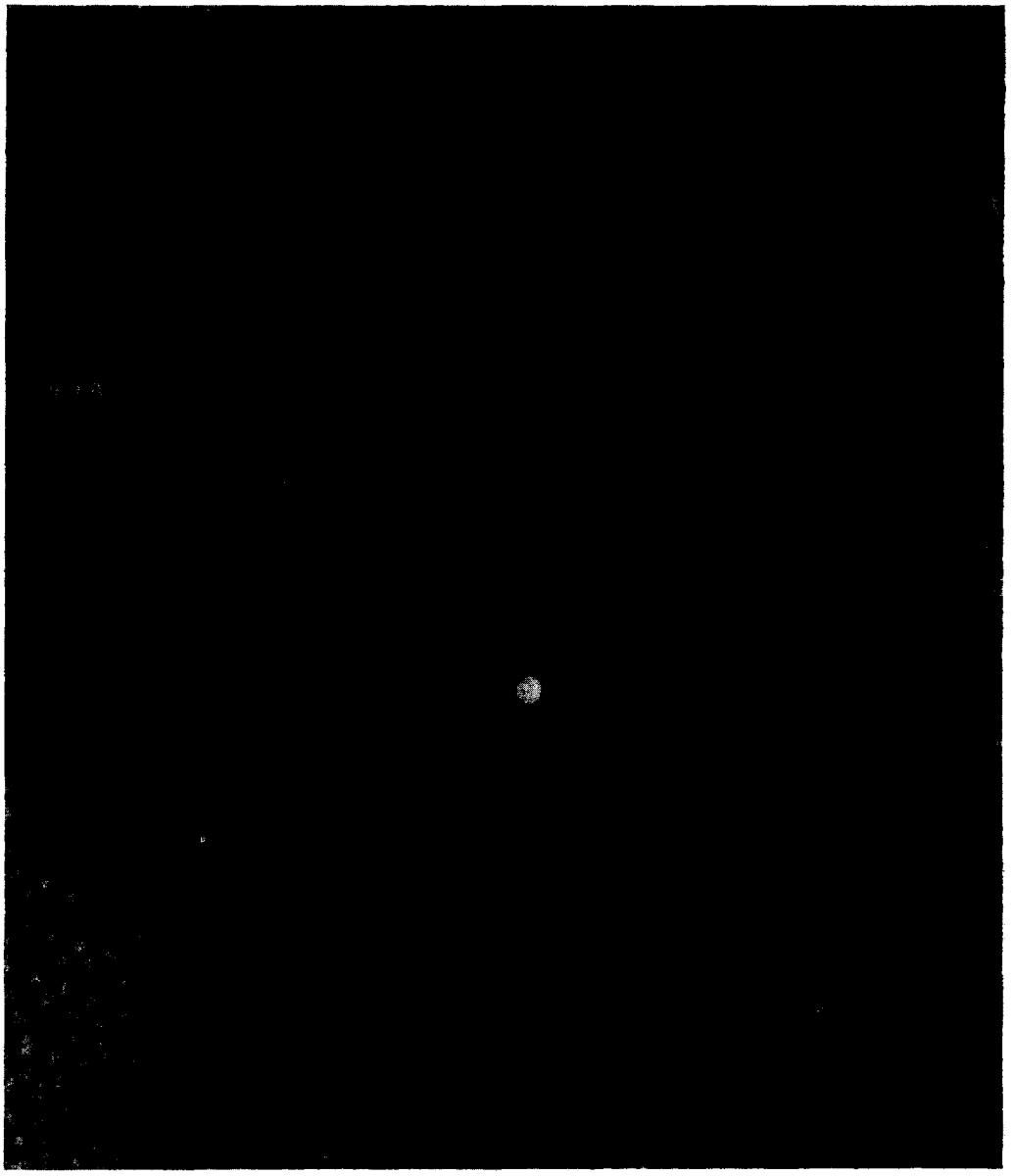

FIG. 6. Lattice image of $Tb_{11}O_{20}$. Bright field.

where the specimen thickness may be more favorable and an almost layer-like appearance obtains. An optical enhancement of this image is given in Fig. 7. The positioning of these light spots in the unit cell is that deduced above for the structure of $Tb_{11}O_{20}$ (Fig. 4). It is by no means suggested that the vacancies are imaged directly but the periodic modification which they impose on the potential field is clearly seen. The confirmation of these images by *n*-beam calculations is in progress.

Acknowledgment

It is a pleasure to credit the United States Atomic Energy Commission for support of this work. K.-H. Lau and A. T. Lowe gave valuable assistance in some

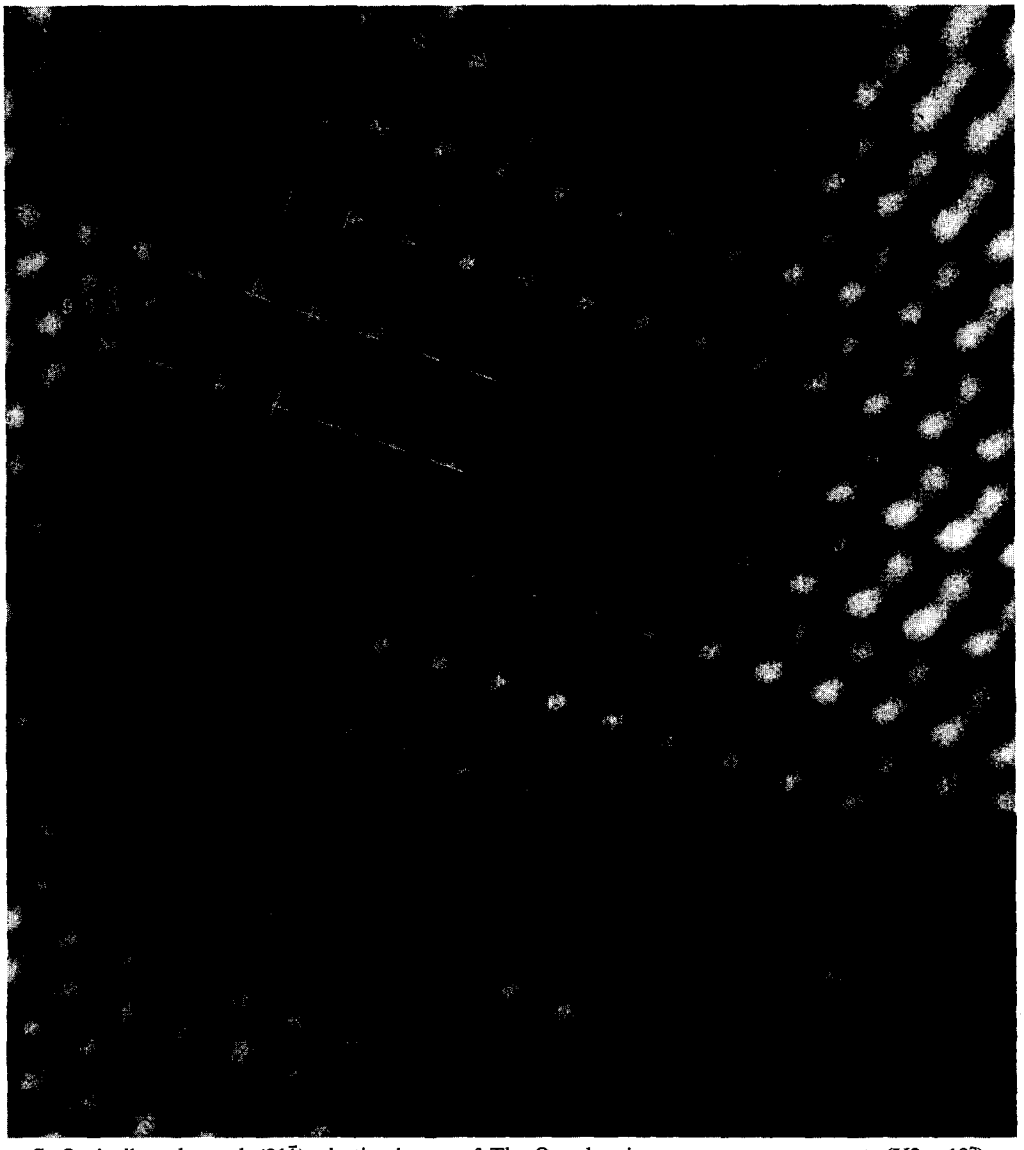

FIG. 7. Optically enhanced $\langle 21\bar{1}\rangle_F$ lattice image of $Tb_{11}O_{20}$ showing vacancy arrangement. (X2 × 10^7).

specimen preparation. Helpful conversations with J. M. Cowley, M. Lundberg and A. J. Skarnulis are also acknowledged.

References

1. B. G. HYDE AND L. EYRING, "Rare Earth Research III" (L. Eyring, Ed.), p. 623, Gordon and Breach, New York, 1965.
2. J. O. SAWYER, B. G. HYDE, AND L. EYRING, *Bull. Soc. Chim.* Franc., 1190 (1965).
3. M. Z. LOWENSTEIN, L. KIHLBORG, K. H. LAU, J. M. HASCHKE, AND L. EYRING, *NBS Spec. Pub.* **364**, 343 (1972).
4. J. M. COWLEY AND S. IIJIMA, *Z. Naturforsch.* **27a**, 445 (1972).
5. R. MARKHAM, *In* "Methods in Virology, IV" (M. Maramorosch and H. Koprowski, Eds.), p. 503, Academic Press, New York, 1968.
6. L. Eyring AND B. HOLMBERG, "Advances in Chemistry Series, Number 39," p. 46 (1963).
7. N. C. BAENZIGER, H. A. EICK, H. S. SCHULDT, AND L. EYRING, *J. Amer. Chem. Soc.* **83**, 2219 (1961).
8. S. F. BARTRAM, *Inorg. Chem.* **5**, 749 (1966).
9. A. T. LOWE AND L. EYRING, unpublished data.
10. M. R. THORNBER, D. J. M. BEVAN, AND J. GRAHAM, *Acta Cryst.* **B24**, 1183 (1968).